Functional Connectivity of Default Mode Network Components: Correlation, Anticorrelation, and Causality

Lucina Q. Uddin,[1] **A.M. Clare Kelly,**[1] **Bharat B. Biswal,**[2]
F. Xavier Castellanos,[1]* **and Michael P. Milham**[1]*

[1]*The Phyllis Green and Randolph Cōwen Institute for Pediatric Neuroscience,
New York University Child Study Center, New York, New York*
[2]*Department of Radiology, University of Medicine and Dentistry of New Jersey,
Newark, New Jersey*

Abstract: The default mode network (DMN), based in ventromedial prefrontal cortex (vmPFC) and posterior cingulate cortex (PCC), exhibits higher metabolic activity at rest than during performance of externally oriented cognitive tasks. Recent studies have suggested that competitive relationships between the DMN and various task-positive networks involved in task performance are intrinsically represented in the brain in the form of strong negative correlations (anticorrelations) between spontaneous fluctuations in these networks. Most neuroimaging studies characterize the DMN as a homogenous network, thus few have examined the differential contributions of DMN components to such competitive relationships. Here, we examined functional differentiation within the DMN, with an emphasis on understanding competitive relationships between this and other networks. We used a seed correlation approach on resting-state data to assess differences in functional connectivity between these two regions and their anticorrelated networks. While the positively correlated networks for the vmPFC and PCC seeds largely overlapped, the anticorrelated networks for each showed striking differences. Activity in vmPFC negatively predicted activity in parietal visual spatial and temporal attention networks, whereas activity in PCC negatively predicted activity in prefrontal-based motor control circuits. Granger causality analyses suggest that vmPFC and PCC exert greater influence on their anticorrelated networks than the other way around, suggesting that these two default mode nodes may directly modulate activity in task-positive networks. Thus, the two major nodes comprising the DMN are differentiated with respect to the specific brain systems with which they interact, suggesting greater heterogeneity within this network than is commonly appreciated. *Hum Brain Mapp 30:625–637, 2009.* © 2008 Wiley-Liss, Inc.

Key words: fMRI; resting state network; ventromedial prefrontal cortex; posterior cingulate; precuneus; Granger causality; effective connectivity; attention; self; social cognition

---

INTRODUCTION

The repeated observation that the ventral medial prefrontal cortex (vmPFC) and posterior cingulate cortex (PCC) paradoxically exhibit high levels of activity during resting baseline and decreases in activity during externally oriented cognitive tasks led to the characterization of these regions as belonging to a "default mode network" (DMN) [Esposito et al., 2006; Fransson, 2006; Gusnard et al., 2001a; McKiernan et al., 2003; Raichle et al., 2001]. Originally proposed as a system for evaluating "information broadly arising in the external and internal milieu" [Raichle et al., 2001], the network has since been posited to underlie a variety of functions. The DMN has been linked to episodic memory [Greicius and Menon, 2004] and memory consolidation [Miall and Robertson, 2006] in some studies, and social [Iacoboni et al., 2004; Uddin et al., 2005] or self-related processes [Buckner and Carroll, 2007; Gusnard et al., 2001a; Wicker et al., 2003] in others. Still others associate default mode function with more general processes such as stimulus-independent [Mason et al., 2007] or task-unrelated thought [McKiernan et al., 2006]. Though it is possible that one comprehensive theory will arise explaining the network's ability to support such a diverse array of functions, the greater likelihood is that the DMN consists of functionally differentiable subdivisions or subnetworks.

Evidence for functional differentiation within the DMN comes from task-based activation studies, where vmPFC and PCC are often reported to act independently across a wide array of cognitive tasks. In the emerging social cognitive neuroscience literature, one of the most ubiquitous findings is the link between the ventral division of medial frontal cortex and tasks involving mentalizing, or reflecting on mental states of others [Gilbert et al., 2006], especially others perceived as similar to the self [Mitchell et al., 2006]. Similarly, vmPFC is often implicated in perception and judgments of other people [Mitchell et al., 2002]. This region is also involved in representing self-knowledge [Macrae et al., 2004] or self-referential processing [D'Argembeau et al., 2005]. Activity in the posterior cingulate and precuneus, on the other hand, is more commonly associated with episodic memory retrieval [Lou et al., 2004; Lundstrom et al., 2005] and visuo-spatial imagery [Cavanna and Trimble, 2006]. On the basis of these functional distinctions, one would predict that the anterior and posterior regions comprising the DMN should show differences in their interactions with other networks.

Recent advances in fMRI analysis methods have enabled the study of spontaneous neural activity and network interactions at rest (e.g., data collected while subjects engage in a low-level task such as fixating on a central cross). Since the discovery by Biswal and colleagues that spontaneous fluctuations during rest were coherent within the somatomotor system [Biswal et al., 1995], several researchers have confirmed that many of the networks known to be engaged during various cognitive tasks are also identifiable during resting states (e.g., dorsal and ventral attention systems [Fox et al., 2006], hippocampal memory systems [Vincent et al., 2006]).

Intriguingly, functional connectivity measures at rest have also shown a tight coupling between the DMN and "task-positive" networks, manifest as strong negative correlations or "anticorrelations" [Fox et al., 2005]. While strong positive correlations between regions indicate that those regions are typically comodulated during task performance, anticorrelations between networks indicate that the networks are temporally modulated in opposite directions [Fox et al., 2006]. Anticorrelations may therefore reveal key aspects of functional organization of the brain, as they are thought to represent the dichotomy between increased brain activity in regions supporting execution of a task and decreased brain activity in regions involved in unrelated processes [Fox et al., 2005]. It has been suggested that anticorrelations represent a "division of labor" between networks with seemingly opposite functions [Fransson, 2006]. The anticorrelation between the DMN and task-positive frontoparietal networks, for example, may reflect the dichotomy between tasks requiring introspectively oriented vs. extrospectively oriented attentional modes [Fransson, 2005]. Such competitive relationships can significantly impact behavioral performance. For example, failure to suppress activity in the posterior node of the DMN results in attentional lapses [Weissman et al., 2006], and the competitive relationship between the DMN and its anticorrelated network influences behavioral performance [Kelly et al., 2007].

Despite considerable interest in the DMN and its relationship with other networks, little is known about possible heterogeneity within the network itself. A previous study of resting-state functional connectivity in the DMN reported strong coupling between the vmPFC and PCC, with subtle differences between the two networks. Though analysis of the differences between the two networks was not the main focus of that study, the authors did report that a seed placed in the PCC region "provided a far more complete match with the hypothesized DMN" [Greicius et al., 2003], suggesting variability within the DMN. Similarly, approaches employing independent component analysis (ICA), or probabilistic ICA (PICA) typically capture the entire DMN as a single major component [De Luca et al., 2006]. One report of ICA separation of anterior and posterior DMN components exists, though the implications were not discussed [Damoiseaux et al., 2006]. Accordingly, previous work has typically characterized the vmPFC and PCC as belonging to a single network. However, whether the entire DMN functions as a single unit, or whether each DMN node has a specific functional role remains unknown. Additionally, the directionality of influence of each DMN node on its anticorrelated network has not been investigated.

Here, we used a seed-based correlation analysis to determine the functional connectivity of vmPFC and PCC at rest. We hypothesized that seeding these regions individually would reveal important differences in resting-state

functional connectivity between the two. We were particularly interested in examining the networks negatively correlated with each individual seed, given our preliminary findings that the strength of the coupling between the DMN and its antinetwork is related to behavioral variability [Kelly et al., 2007]. To understand the "effective connectivity" [Friston, 1994; Goebel et al., 2003; Roebroeck et al., 2005] between each network and its anticorrelated counterpart, we also computed Granger causality probabilities [Granger, 1969] as an indirect measure of the directionality of causal influence between the networks.

METHODS

Subjects

Twenty-six (average age = 28.4 ± 8.5, nine females) healthy, right-handed subjects participated in the study. All subjects were free of psychiatric disorders or history of head trauma. Participants signed informed consent after the experimental procedures were explained, prior to scanning, and received monetary compensation. The study complied with the Code of Ethics of the World Medical Association (Declaration of Helsinki) and was IRB approved at New York University and the NYU School of Medicine.

fMRI Data Acquisition and Analysis

Functional images were acquired on a Siemens Allegra 3-Tesla scanner using an EPI gradient echo sequence (TR = 2,000 ms; TE = 25 ms; Flip angle = 90°, 39 slices, matrix 64 × 64; FOV = 192 mm; acquisition voxel size 3 mm × 3 mm × 3 mm) while subjects were instructed to rest with eyes open. For each participant, 197 contiguous EPI functional volumes were acquired, resulting in a 6 min 38 s scan. A subset of these data provided the basis for mapping anterior cingulate functional connectivity in a separate analysis [Margulies et al., 2007]. During this functional scan, the word "Relax" was projected in white font against a black background. A T1-weighted anatomical image was also acquired for registration purposes (MP-RAGE, TR = 2,500 ms; TE = 4.35 ms; TI = 900 ms; Flip angle = 8°; 176 slices; FOV = 256 mm).

A schematic of the data processing stream is shown in Figure 1a. Data preprocessing was completed using FSL (Oxford Centre for Functional Magnetic Resonance Imaging of the Brain Software Library, www.fmrib.ox.ac.uk). Image preprocessing comprised slice-timing correction for interleaved acquisition (using Fourier-space time series phase-shifting), motion correction (using a 6 parameter affine transformation), spatial smoothing (using a Gaussian kernel of FWHM 6 mm), and temporal bandpass filtering (highpass temporal filtering: Gaussian-weighted least-squares straight line fitting, with sigma = 100.0s; Gaussian lowpass temporal filtering HWHM 2.8s). These temporal filtering parameters were selected based on prior work
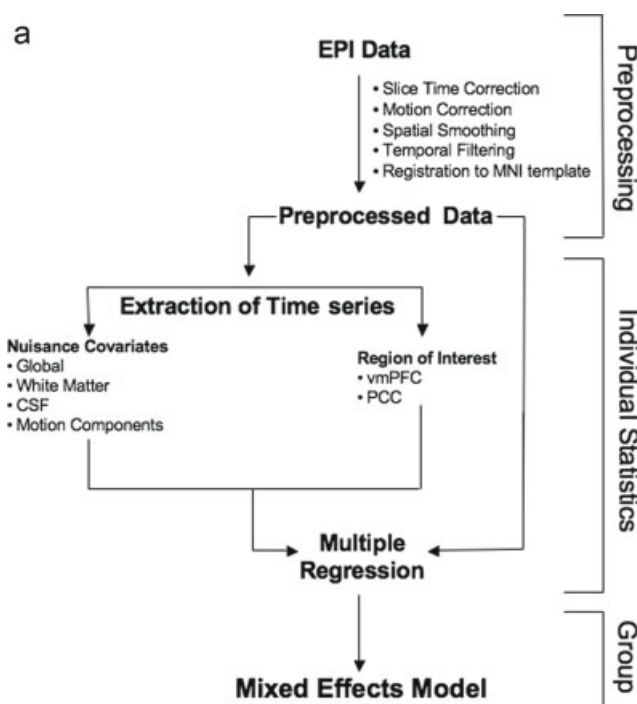

Figure 1.

(a) Diagram of data processing steps. (b) Locations of seeds used for correlation analysis (vmPFC Talairach coordinates = 2, 54, −3; PCC Talairach coordinates = −2, −51, 27).

demonstrating that spontaneous fluctuations upon which functional connectivity analyses are based exist in the range of 0.01–0.1 Hz [Biswal et al., 1995]. Inclusion of a lowpass filter facilitated removal of high-frequency noise unrelated to our signals of interest. As a final preprocessing step, each individual's time series was normalized by registration to the Montreal Neurological Institute (MNI) template, with 3 mm resolution, using a 6 degrees-of-freedom affine transformation.

For the functional connectivity analysis, we created two spherical "seed" ROIs (ten 3 mm × 3 mm × 3 mm voxels, volume = 270 mm^3) centered in vmPFC (Brodmann area 10) and PCC (Brodmann area 31), using Talairach coordinate locations from previous work [De Luca et al., 2006] (Fig. 1b). These Talairach coordinates were first converted to MNI space using the algorithm implemented in the Matlab script tal2mni.m (http://imaging.mrc-cbu.cam.ac.uk/imaging/MniTalairach). The ROIs were used to extract an average hemodynamic time series for each location, and for each subject, by applying each ROI mask to the preprocessed time series, and averaging across all voxels within the ROI. We then carried out a multiple regression analysis (using the GLM as implemented in FEAT), with the vmPFC and PCC seed time series regressors and nuisance covariates (global signal, cerebrospinal fluid, white matter). Specifically, the GLM included the three nuisance (global, csf, white matter) and the two seed (vmPFC, PCC) time series. Using Gramm Schmidt orthogonalization as implemented in FSL, vmPFC was orthogonalized with respect to global, csf, white matter, and PCC. PCC was orthogonalized with respect to global, csf, white matter, and vmPFC. The global signal, thought to reflect a combination of physiological processes (such as cardiac and respiratory fluctuations) and scanner drift, was included in the GLM to minimize the influence of such factors [Birn et al., 2006; Gavrilescu et al., 2002; Macey et al., 2004]. An analysis of the data without global signal correction is presented in supplementary materials (Supplementary Fig. 1). Orthogonalizing the two seed ROIs with respect to each other effectively leaves out signal that covaries in the two regions. This allowed examination of differences between the anterior and posterior nodes, as their commonalities have been documented in previous reports. This analysis identified voxels that were uniquely functionally connected to each ROI, as well as those that were members of the corresponding anticorrelated networks. Group-level analyses were carried out using FLAME, a mixed-effects model in FSL, to produce thresholded Z-score maps of voxels positively and negatively correlated with each ROI. We will refer to voxels positively correlated with the vmPFC seed as the vmPFC+ network, and voxels negatively correlated with the vmPFC seed as the vmPFC− network. Similarly, voxels positively correlated with the PCC seed belong to the PCC+ network, and voxels negatively correlated with the PCC seed are part of the PCC− network. Corrections for multiple comparisons were carried out at the cluster level using Gaussian random field theory (min Z > 2.3; cluster significance: $P < 0.05$, corrected).

Granger Causality Analysis

Initial analysis of fMRI data (filtered for temporal drift, high-frequency noise and nuisance covariates) using a modified general linear model indicated activity in 4 networks (vmPFC+, vmPFC−, PCC+, and PCC−). Granger causality methods were used to assess dynamic interac-tions between these cortical regions. Granger causality between two regions can be defined as the extent to which the data from one region at one point in time improves the prediction of another region's data at a later point in time [Goebel et al., 2003]. We used this analysis to evaluate causal influences between networks by measuring the extent to which signal changes in one region reliably preceded those in other regions at later points in time, permitting characterization of the strength and direction of influence between discrete brain regions [Goebel et al., 2003; Roebroeck et al., 2005]. For this analysis, the mean time series of all voxels within each network (vmPFC+, vmPFC−, PCC+, PCC−) was calculated.

Granger analysis was performed using code written in MATLAB, as follows. (1) For each pair of networks, the mean time series from each network was fit using a full vector autoregressive model, which took both time series into account. Briefly, in a vector autoregressive process the time series datasets assume that the current time point is functionally related to its N previous time points. For this study, a 5th order vector autoregressive process was used for each of the four networks. (2) From one of the two time series in a pair, five sequential time points (10 s) were randomly omitted and the effect on predicting the output was calculated. The time series with omitted time points is referred to as the "sub-model" (suboptimal model). Ten seconds were omitted to account for the delay in the hemodynamic response which occurs after a neuronal response [Lee et al., 1995]. The selection of 10 s was based on the observation that delay between regions has been shown to be as large as 8 s [Saad et al., 2001]. (3) Sub-model fits were then carried out for each time series dataset compared with the other time series datasets. Time point omission from one regional time series permitted characterization of its influence on other subsequent time points in other regional time series. The significance level for each of them was tabulated for within group analysis.

The Granger analysis we performed used F-statistics to test whether lagged information on a time series (variable) y provided any statistically significant information about another time series (variable) x in the presence of lagged x. If not, then "y did not cause x." The vector autoregression model we used assumed an autoregressive lag length p, and estimated the following unrestricted equation by ordinary least squares (OLS):

$$x(t) = c1 + \sum_{i=1}^{p} a(i)x(t-i) + \sum_{i=1}^{p} b(i)y(t-i) + u(t) \quad (1)$$

where $x(t)$ and $y(t)$ are the two time series being evaluated for causality, t is the current time point, $a(i)$ and $b(i)$ are the linear prediction variables for x and y, u is the error of the fit, and p is the lag length.

The F-statistic tested the null hypothesis (Ho: b(1) = b(2) = b(3) = $\cdots$ b(p) = 0) using the following simplification of Eq. (1):
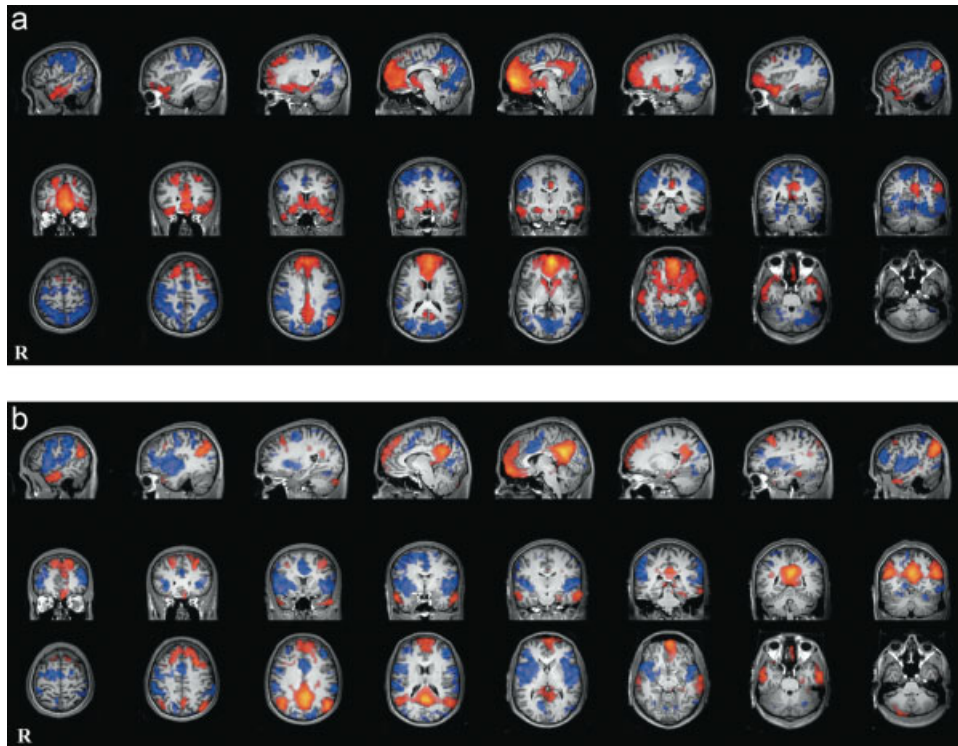
Figure 2.

Positive and negative correlations with each seeded region. (**a**) vmPFC (orange) and its anticorrelated network (blue). (**b**) PCC (orange) and its anticorrelated network (blue).

$$x(t) = c1 + \sum_{i=1}^{p} g(i)x(t-i) + e(t) \qquad (2)$$

where $x(t)$ is the time series being evaluated for causality, t is the current time point, $g(i)$ is the linear prediction variable for x, e is the error in fit, and p is the lag length.

If the F-test

$$F_{y,x} = \frac{\left(\sum_{i=1}^{T} e(i) - \sum_{i=1}^{T} u(i)\right) \Big/ p}{\left(\sum_{i=1}^{T} u(i)\right) \Big/ (T - 2p - 1)} \qquad (3)$$

(where T is the total number of time-points and p is the lag length) was greater than tabular significance values, then the null hypothesis (y does not cause x) was rejected, and the alternative "y causes x," is accepted.

This procedure was performed on the data from all networks and their influences on all other networks were computed. Each time series dataset was modeled and the sub-model was compared against the other time series datasets. Sub-model fits and directional causality were then tabulated for each of the time series datasets. This process was repeated until all possible combinations were obtained, thus mutual directional causality was analyzed between all four networks, resulting in twelve tests. Model diagnostic tests and resulting significance levels were estimated from the sub-model fit matrix [Goebel et al., 2003]. Directed influences between the different regions were calculated for the significance level $P < 0.10$.

RESULTS

Positively-Correlated Networks (vmPFC+, PCC+)

The vmPFC seed correlation analysis revealed that in addition to highly correlating with precuneus/posterior cingulate, activity in this seed correlated with several frontal regions including right medial frontal, left superior frontal, bilateral inferior frontal, and bilateral middle frontal gyrus. Additionally, bilateral middle temporal, and right angular gyrus correlated with activity in this seed. Bilateral parahippocampal gyri and right cingulate were also correlated with the vmPFC seed (Fig. 2a, Table I).

The posterior cingulate seed was correlated with bilateral medial frontal cortices, precuneus, and bilateral posterior parietal cortices (right and left angular gyrus). Several frontal regions also correlated with the PCC seed, namely bilateral middle frontal, bilateral superior frontal, and left inferior frontal gyrus. Temporal regions included bilateral

TABLE I. vmPFC Seed: Talairach coordinates of regions positively correlated

Region	Peak activation Z-score	x	y	z	Brodmann area
Medial frontal gyrus (R)	11.34	6	57	0	11
Superior frontal gyrus (L)	7.93	0	57	27	9
Inferior frontal gyrus (R)	6.51	33	12	−18	47
Inferior frontal gyrus (L)	5.74	−30	15	−18	47
Precuneus (R)	5.63	6	−54	30	7
Middle temporal gyrus (R)	5.39	63	−18	−18	20
Angular Gyrus (R)	5.26	51	−72	36	39
Cingulate Gyrus (R)	5.08	3	−18	33	23
Middle temporal gyrus (L)	5.07	−60	−27	−15	21
Middle temporal gyrus (R)	5.05	51	12	−39	21
Parahippocampal gyrus (R)	4.99	30	−30	−12	36
Middle temporal gyrus (L)	4.98	−51	9	−33	21
Parahippocampal gyrus (L)	4.98	−27	−18	−15	36
Middle frontal gyrus (R)	4.87	30	24	48	8
Middle frontal gyrus (L)	4.41	−33	54	−9	10

inferior temporal and right superior temporal gyrus. The right fusiform gyrus and right postcentral gyrus also showed correlated activity with this seed (Fig. 2b, Table II).

Negatively-Correlated Networks (Antinetworks, vmPFC−, PCC−)

Activity in the vmPFC network was anticorrelated with extrastriate visual areas (left superior occipital gyrus, right middle occipital gyrus, right lingual gyrus, bilateral fusiform gyrus, bilateral cuneus) and attention networks (bilateral inferior parietal lobule, right inferior frontal gyrus, left middle frontal gyrus, left medial frontal gyrus). Additional anticorrelations were seen with anterior and posterior portions of right cingulate gyrus and precuneus as well as bilateral inferior temporal gyrus, right middle temporal gyrus, right postcentral gyrus, and left insula (Fig. 2a, Table III).

The anticorrelation analysis for the PCC seed also showed extrastriate visual areas (bilateral lingual gyrus, bilateral cuneus, bilateral middle occipital gyrus) and parietal networks (bilateral inferior parietal lobule, bilateral postcentral gyrus). There were also anticorrelations with left anterior cingulate and left medial frontal gyrus, lateral prefrontal (bilateral middle and superior frontal gyri, bilateral insula, left inferior frontal gyrus), and lateral temporal networks (bilateral superior temporal gyrus, bilateral middle temporal gyrus) as well as parts of left precuneus (Fig. 2b, Table IV).

Direct Comparisons Between Networks

To verify differences between the two positive networks and the two negative networks, direct contrasts between the vmPFC+ and PCC+ networks were computed on a voxel-wise basis ($Z > 2.3$, $P < 0.05$, corrected). Masking

TABLE II. PCC Seed: Talairach coordinates of regions positively correlated

Region	Peak activation Z-score	x	y	z	Brodmann area
Posterior cingulate gyrus (R)	11.44	3	−54	27	31
Angular gyrus (R)	7.17	51	−66	33	39
Medial frontal gyrus (R)	7.02	3	60	−12	11
Angular gyrus (L)	6.98	−42	−57	30	39
Medial frontal gyrus (L)	6.06	−3	54	24	9
Inferior temporal gyrus (R)	6.02	69	−9	−21	21
Middle frontal gyrus (R)	5.83	27	24	45	8
Inferior temporal gyrus (L)	5.69	−54	−12	−24	20
Superior frontal gyrus (R)	5.57	21	42	51	8
Superior temporal gyrus (R)	4.99	57	15	−33	38
Superior frontal gyrus (L)	4.88	−12	42	51	8
Fusiform gyrus (R)	4.37	33	−39	−18	20
Superior frontal gyrus (R)	3.80	24	66	0	10
Inferior frontal gyrus (L)	3.73	−30	24	−21	47
Postcentral gyrus (R)	3.70	30	−24	33	2
Middle frontal gyrus (L)	3.62	−42	18	36	9

TABLE III. vmPFC seed: Talairach coordinates of regions negatively correlated

Region	Peak activation Z-score	x	y	z	Brodmann area
Inferior parietal lobule (L)	6.59	−39	−48	51	40
Superior occipital gyrus (L)	5.79	−30	−81	27	19
Precuneus (R)	5.59	27	−54	51	7
Inferior parietal lobule (R)	5.35	63	−42	39	40
Inferior parietal lobule (R)	5.34	42	−45	45	40
Cuneus (L)	5.30	−6	−78	15	18
Fusiform gyrus (L)	5.13	−48	−45	−24	36
Cuneus (R)	5.08	9	−78	6	18
Cuneus (R)	5.06	15	−93	18	18
Middle frontal gyrus (L)	5.05	−51	6	48	6
Middle occipital gyrus (R)	5.03	33	−81	15	19
Lingual gyrus (R)	4.77	21	−72	0	18
Inferior frontal gyrus (R)	4.71	60	6	33	6
Postcentral gyrus (R)	4.70	54	−18	54	3
Inferior temporal gyrus (L)	4.65	−54	−60	−15	37
Fusiform gyrus (L)	4.63	−27	−60	−6	19
Middle temporal gyrus (R)	4.48	51	−75	9	39
Medial frontal gyrus (L)	4.48	−18	3	54	6
Inferior temporal gyrus (R)	4.42	66	−60	−9	37
Middle occipital gyrus (R)	4.28	48	−69	−9	19
Cingulate Gyrus (R)	4.22	9	6	42	32
Cingulate gyrus (R)	3.51	18	−33	36	31
Insula (L)	3.13	−45	9	15	13

was performed to determine regions specifically connected to each seed. For example, areas common to the vmPFC+ network (Fig. 2a) and the vmPFC > PCC contrast are unique to the vmPFC seed. These regions encompass mainly bilateral frontal and temporal gyri (Fig. 3a, Supplementary Table I). A similar mask shows the regions

TABLE IV. PCC seeds: Talairach coordinates of regions negatively correlated

| Region	Peak activation Z-score	x	y	z	Brodmann area
Superior temporal gyrus (L)	6.42	−39	6	−15	38
Superior temporal gyrus (L)	6.37	−57	9	3	22
Insula (R)	6.26	45	12	−3	47
Cingulate gyrus (L)	5.56	−3	18	30	32
Inferior frontal gyrus (L)	5.53	−45	3	18	44
Middle frontal gyrus (R)	5.32	48	39	30	46
Medial frontal gyrus (L)	5.23	−3	9	51	6
Inferior parietal lobule (R)	5.07	66	−33	39	40
Inferior parietal lobule (L)	5.05	−57	−39	54	40
Middle temporal gyrus (R)	4.99	66	−60	−3	37
Precuneus (L)	4.94	−18	−87	42	19
Cuneus (R)	4.71	21	−90	30	19
Middle frontal gyrus (L)	4.70	−42	−3	63	6
Inferior parietal lobule (L)	4.62	−69	−24	20	40
Postcentral gyrus (R)	4.59	60	−39	57	40
Cuneus (L)	4.54	−12	−75	3	18
Inferior parietal lobule (L)	4.53	−57	−33	24	40
Superior frontal gyrus (L)	4.38	−30	48	27	9
Postcentral gyrus (L)	4.04	−6	−57	69	7
Middle occipital gyrus (R)	3.97	42	−75	3	19
Middle occipital gyrus (R)	3.93	48	−90	18	19
Superior temporal gyrus (R)	3.90	66	−21	12	42
Middle frontal gyrus (R)	3.82	24	0	63	6
Middle temporal gyrus (L)	3.77	−42	−78	15	19
Lingual gyrus (R)	3.70	21	−69	−3	19
Cuneus (R)	2.94	6	−99	−3	18
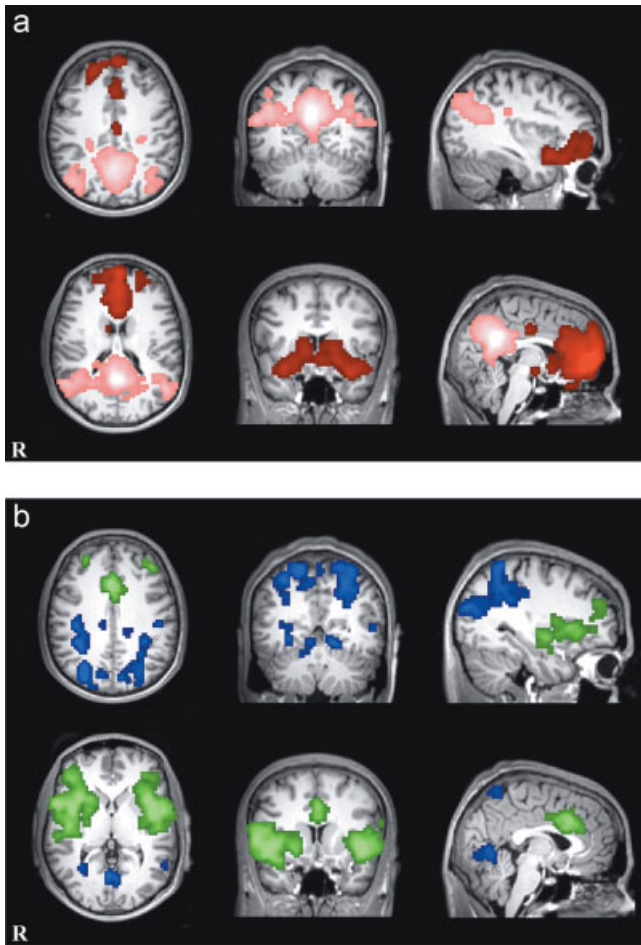
Figure 3.

Direct comparisons between positive and negative networks for each seed. (**a**) vmPFC (red) and PCC (pink) positively correlated networks. (**b**) vmPFC (blue) and PCC (green) negatively correlated networks.

unique to the PCC seed, mostly lateral parietal cortices (PCC+ network masked with PCC > vmPFC, Fig. 3a, Supplementary Table II). Direct comparisons between the networks negatively correlated with each of the seeds were also computed. The vmPFC− network was quantified with the following mask: vmPFC− masked with PCC > vmPFC. This revealed that several regions of the precuneus, parietal lobules, middle temporal, and occipital gyri are unique to the vmPFC antinetwork (Fig. 3b, Supplementary Table III). Lastly, PCC− masked with vmPFC > PCC shows that anterior cingulate, insula, lateral prefrontal regions, and bilateral superior temporal gyri are unique to the PCC negative network (Fig 3b, Supplementary Table IV).

Relationships Between Networks

We examined the relationship between coupling of activity in the DMN subnetworks (vmPFC+, PCC+), and that
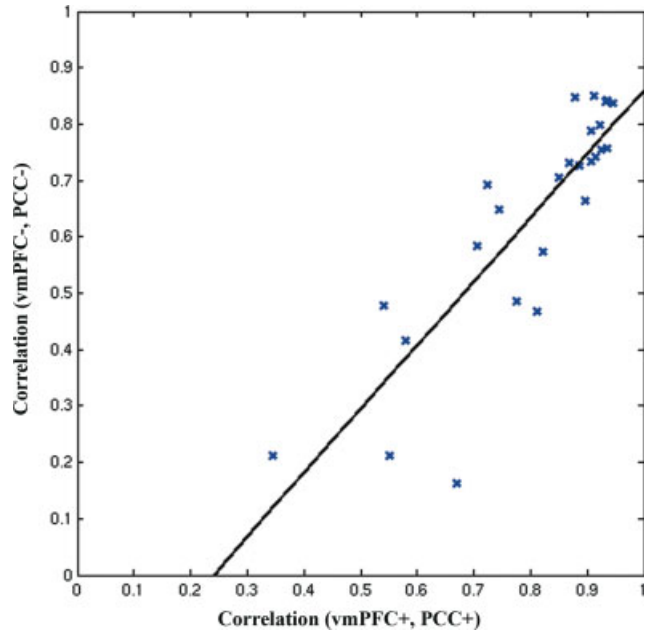

Figure 4.

Correlation between DMN components and antinetworks.

in the two antinetworks (vmPFC−, PCC−). As demonstrated in Figure 4, the more tightly coupled the two DMN subnetworks for a given subject, the more tightly coupled the two DMN antinetworks ($r = 0.83$, $z_r = 1.19$, $P = 2.35 \times 10^{-8}$).

Table V shows significant Granger causality between networks at the group level. Granger causality analyses showed influences between each pair of networks. Most notably, the vmPFC+ and PCC+ networks significantly influenced their respective antinetworks (Table V). This suggests that the two default mode nodes may causally influence activity in their respective antinetworks. The per-

TABLE V. Granger causality probabilities predicting influences between positively correlated (+) and negatively correlated (−) networks

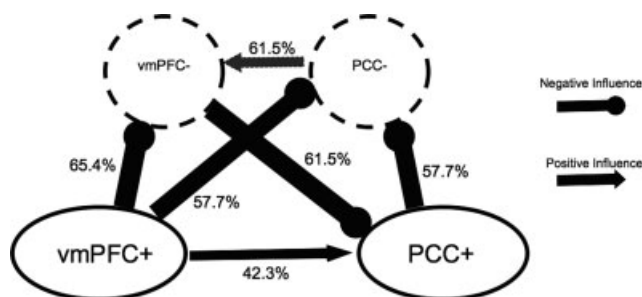| Network	Predicts values in:	% Subjects with significant Granger causality	Binomial test significance
vmPFC+	vmPFC−	65.4	1.2×10^{-11}
vmPFC+	PCC−	57.7	2.4×10^{-9}
vmPFC+	PCC+	42.3	1.6×10^{-5}
PCC+	vmPFC−	3.8	0.2
PCC+	PCC−	57.7	2.4×10^{-9}
PCC+	vmPFC+	11.5	0.2
vmPFC−	vmPFC+	11.5	0.2
vmPFC−	PCC+	61.5	1.9×10^{-10}
vmPFC−	PCC−	15.4	0.1
PCC−	vmPFC+	19.2	0.1
PCC−	PCC+	3.8	0.2
PCC−	vmPFC−	61.5	1.9×10^{-10}

Figure 5.
Granger causality results. Significant relationships between DMN components and antinetworks. The percentage values indicate proportion of subjects showing significant relationship at $P < 0.1$. As indicated by the binomial test, a significant relationship at that threshold in 30% or more subjects is significant at $P < 0.01$.

centage values indicate proportion of subjects showing significant relationship at $P < 0.10$. This more lenient within-subject threshold was employed due to the number of points included in the Granger causality analysis. As indicated by the binomial test, a significant relationship at that threshold in 30% or more subjects is significant at $P < 0.01$ (see Fig. 5).

DISCUSSION

Using seed-based regression analyses of resting state data, we individually assessed functional connectivity of the anterior (vmPFC) and posterior (PCC) components of the DMN. We found that the anticorrelated networks associated with the anterior and posterior seeded regions appear to be dissociable. The functional significance of these anticorrelated networks is unknown, although they are posited to serve a differentiating role segregating neural processes subserving competing representations or opposite goals [Fox et al., 2005]. The presence of such anticorrelations is consistent with a recently published computational model of functional connectivity across multiple time scales [Honey et al., 2007]. Previous studies have demonstrated anticorrelations between lateral prefrontal ROIs showing task-related increases, and the DMN, suggesting the possibility of inhibitory interactions between these and default mode regions [Greicius et al., 2003]. Such anticorrelations might be more accurately referred to as manifestations of *ensemble inhibition*, a term that refers to interactions between brain areas as defined by patterns of covariation, rather than individual neurons [Nyberg et al., 1996]. This competitive relationship between the DMN and task-positive networks has consequences for behavioral performance, as recently demonstrated [Kelly et al., 2007]. Previous work has hinted at functional differentiation between the anterior and posterior nodes of the DMN, as failure to suppress PCC activity is associated with attentional lapses [Weissman et al., 2006]. The anti-

correlated networks we found for each DMN component were strikingly different for the two seeded regions. Below we discuss the known functions of each of the networks revealed by this analysis and implications for theories of default mode function.

Discussion of Areas Correlated With vmPFC and PCC

The seeds placed in vmPFC and PCC showed positive correlations with each other, consistent with previous functional connectivity analyses of these two regions [Fox et al., 2005; Greicius et al., 2003; Hampson et al., 2006]. The regions connected to each of the individual seeds also followed the expected pattern. The vmPFC seed was more strongly positively correlated with adjacent frontal and temporal regions, whereas the PCC seed was more correlated with nearby mid- and lateral parietal regions. Our analysis revealed patterns of connectivity for both of these regions that is consistent with what is known about their anatomical connectivity [for review of vmPFC see Amodio and Frith, 2006; for review of PCC see Cavanna and Trimble, 2006].

Our approach of separately seeding the vmPFC and PCC and orthogonalizing each network with respect to the other revealed the novel finding that each network has a unique variance capable of predicting distinct patterns of interactions throughout the DMN. ICA methods of identifying the DMN [Damoiseaux et al., 2006; De Luca et al., 2006] typically capture only the common variance, and, thus, miss the subtle differences in functional connectivity we report here. Previous seed-based ROI approaches have also overlooked potential differences between the networks. A major difference between our results and a previous study by Fox et al. is that they perform a conjunction analysis in which voxels were only included if they were significantly correlated or anticorrelated with five of the six seed regions, thus, biasing the report towards finding commonalities between networks. Our focus, instead, was to identify potential differences between the networks; thus, our methods produce understandably contrasting results [Fox et al., 2005]. We show that orthogonalizing the time courses of ROIs with respect to each other prior to multiple regression reveals differences between them that other approaches miss.

Discussion of Areas Anticorrelated With vmPFC

Areas comprising the anticorrelated network for vmPFC resemble those most commonly activated in studies of visual and spatial attention, namely superior/inferior parietal and extrastriate cortices [Coull and Nobre, 1998; Nobre et al., 1997]. This anticorrelated network resembles the "task-positive" network identified using similar methods by other groups [Fox et al., 2005; Fransson, 2005]. The fact that such networks are anticorrelated with vmPFC suggests that they are coupled to vmPFC activity. Our

Granger causality analyses suggest that the direction of causality is stronger from vmPFC+ to vmPFC− than vice versa. As previously noted, the vmPFC is often associated with mentalizing, evaluative, and self-referential processing. Such processes typical require attention to be diverted away from stimuli in the external environment and redirected to monitoring one's own or another's mental state. It would thus make sense for these two networks to have an antagonistic relationship, to allow for activation of one or the other as task demands require, but not both simultaneously.

Discussion of Areas Anticorrelated With PCC

The networks found to be anticorrelated with the PCC seed resembled prefrontal-based motor planning and control circuits. Much of the circuitry revealed here overlaps with parts of the human mirror neuron network (inferior frontal gyrus and superior temporal gyrus) involved in action observation and execution [Rizzolatti and Craighero, 2004]. In addition, the insula is strongly present in the PCC− network. This region has previously been shown to act in concert with the human mirror neuron system during imitation and observation of emotions (e.g., empathy) [Carr et al., 2003]. Additionally, the anterior cingulate, known to be responsive to affective aspects of empathy for pain [Singer et al., 2004] is anticorrelated with the PCC. That such regions should have an antagonistic relationship with the posterior cingulate suggests the intriguing possibility that we have identified an important locus of interaction between the human mirror neuron system and the DMN. Indeed, the Granger causality results for reveal stronger directionality of influence from PCC+ to PCC−. This antagonistic relationship is consistent with known activation patterns of the two networks: the mirror neuron system shows increases in activity during execution and observation of goal-directed actions [Rizzolatti, 2005], whereas DMN activity is attenuated during goal-directed actions [Gusnard et al., 2001b; Weissman et al., 2006]. The fact that these networks interact in such a way is consistent with theories positing that the DMN and mirror neuron system interact during social and self-related cognition [Uddin et al., 2007].

Interestingly, a recent study has shown correlations between anxiety ratings and intrinsic functional connectivity of an anterior cingulate and insula-based network. The network described in that study closely resembles our PCC− network, and suggests a potential mechanism whereby PCC can regulate activity in this "salience network" [Seeley et al., 2007].

Implications of Granger Causality Findings

Several studies have demonstrated default mode suppression during goal-oriented task performance, with failure to suppress default mode activity being linked to decreased activity in task-relevant regions [Greicius and Menon, 2004] and attentional lapses, or decrements in performance [Weissman et al., 2006]. The present work's finding that the anterior node of the DMN may influence activity in parietal networks provides new insight into the need for default mode suppression during performance of attentionally demanding tasks. More specifically, it suggests that this component of the DMN may directly bias the brain towards a nonattentive state at rest, thus, requiring suppression to release attentional networks during task performance. Further examination of causality during task performance is required to test this hypothesis. While our Granger analysis suggests a directionality to the influence that each network exerts on the other, this method is limited in that modeling only these regions does not take into account the possibility that other common inputs may also exert their influences on these systems.

Despite the need for DMN suppression during task performance, a recent study found that greater coordination within the DMN between vmPFC and PCC nodes was associated with better performance during a working memory task [Hampson et al., 2006]. Though seemingly contradictory, our finding that greater connectivity between vmPFC+ and PCC+ is associated with greater connectivity between vmPFC− and PCC−, suggests that the DMN may actually serve to coordinate activity between the two antinetworks. Though speculative, this suggestion would explain recent findings showing that while the DMN is clearly suppressed during a working memory task, a significant amount of spontaneous signal fluctuations in the DMN persists [Fransson, 2006].

We found that vmPFC+ and PCC+ exert greater influence on vmPFC− and PCC− than the other way around, suggesting that during resting-states, the introspectively-oriented processes attributed to these two regions [Amodio and Frith, 2006; Cavanna and Trimble, 2006] likely dominate. As the two networks (vmPFC+ and PCC+) negatively influence their respective antinetworks, they are in a position to suppress externally oriented attentional focus mediated by regions in the vmPFC− and PCC− networks.

Clinical Implications

Differences in activity of the DMN have been linked to cognitive deficits in a number of clinical populations. To date, abnormalities in the DMN have been demonstrated in individuals with autism spectrum disorders [Kennedy et al., 2006], Alzheimer's disease [Buckner et al., 2005; Greicius et al., 2004; Wang et al., 2006], schizophrenia [Liang et al., 2006; Liu et al., 2006], and attention-deficit/hyperactivity disorder [Tian et al., 2006; Zang et al., 2007]. Application of our method to resting data from these populations may provide greater insights into specifically which region of the default mode (anterior or posterior) is compromised in clinically impaired individuals. Considering ADHD and other clinical populations associated with attentional dysfunction, our findings suggest multiple potential loci of dysfunction associated with the DMN.

Most notably are the possibilities that these disorders may be associated with (1) failure to suppress default mode activity, (2) abnormally greater influence of default mode regions on task-positive networks, or (3) decreased connectivity within the DMN, thus decreasing the coordination of its antinetworks, which are commonly implicated in performance of attentional tasks. Indeed, evidence for decreased connectivity between the anterior and posterior nodes of the DMN in ADHD has recently been demonstrated [Castellanos et al., in press]. It is likely that characterization of each of the anticorrelated networks in these various populations, as described here, will be useful in further describing the underlying neuropathology of such conditions.

Implications for Theories of Functional Significance of Default Mode

There exist various methods for identifying the DMN, ranging from ICA [De Luca et al., 2006], to examination of "task-negative" networks [Fransson, 2006], to large-scale network identification [Bellec et al., 2006]. For the most part, these methods are biased towards consideration of the entire DMN as a cohesive unit. Here, we show that individually seeding the anterior and posterior components of this network reveals important differences in functional connectivity between the two regions. Our approach suggests that there is greater heterogeneity in the DMN than is generally appreciated, particularly among the networks anticorrelated with each DMN component. Which terms (self-related or social cognition, task-unrelated thought, etc.) best describe default mode function remains unsettled. Our analysis here suggests that each component of the DMN may be differentially involved in these processes, and that analyzing each individually will lead to a richer understanding of the functions of the network. We speculate that it is unlikely that the DMN as a whole is involved in many or all of the processes previously ascribed to it. The concept of *neural context*, the idea that the role of a brain region is determined by how it interacts with other regions, is particularly relevant here [McIntosh, 2000]. It may be that the relationship between activity in the DMN and its anticorrelated networks, instead of the DMN itself, is most functionally relevant.

ACKNOWLEDGMENTS

REFERENCES

Amodio DM, Frith CD (2006): Meeting of minds: the medial frontal cortex and social cognition. Nat Rev Neurosci 7:268–277.

Bellec P, Perlbarg V, Jbabdi S, Pelegrini-Issac M, Anton JL, Doyon J, Benali H (2006): Identification of large-scale networks in the brain using fMRI. Neuroimage 29:1231–1243.

Birn RM, Diamond JB, Smith MA, Bandettini PA (2006): Separating respiratory-variation-related fluctuations from neuronal-activity-related fluctuations in fMRI. Neuroimage 31:1536–1548.

Biswal B, Yetkin FZ, Haughton VM, Hyde JS (1995): Functional connectivity in the motor cortex of resting human brain using echo-planar MRI. Magn Reson Med 34:537–541.

Buckner RL, Carroll DC (2007): Self-projection and the brain. Trends Cogn Sci 11:49–57.

Buckner RL, Snyder AZ, Shannon BJ, LaRossa G, Sachs R, Fotenos AF, Sheline YI, Klunk WE, Mathis CA, Morris JC, Mintun MA (2005): Molecular, structural, and functional characterization of Alzheimer's disease: Evidence for a relationship between default activity, amyloid, and memory. J Neurosci 25:7709–7717.

Carr L, Iacoboni M, Dubeau MC, Mazziotta JC, Lenzi GL (2003): Neural mechanisms of empathy in humans: A relay from neural systems for imitation to limbic areas. Proc Natl Acad Sci USA 100:5497–5502.

Castellanos FX, Margulies DS, Kelly AMC, Uddin LQ, Ghaffari M, Kirsch A, Shaw D, Shehzad Z, Di Martino A, Biswal B, Sonuga-Barke EJ, Rotrosen J, Adler LA, Milham MP: Cingulate-precuneus interactions: A new locus of dysfunction in adult attention-deficit/hyperactivity disorder (in press).

Cavanna AE, Trimble MR (2006): The precuneus: A review of its functional anatomy and behavioural correlates. Brain 129(Part 3): 564–583.

Coull JT, Nobre AC (1998): Where and when to pay attention: The neural systems for directing attention to spatial locations and to time intervals as revealed by both PET and fMRI. J Neurosci 18:7426–7435.

D'Argembeau A, Collette F, Van der Linden M, Laureys S, Del Fiore G, Degueldre C, Luxen A, Salmon E (2005): Self-referential reflective activity and its relationship with rest: A PET study. Neuroimage 25:616–624.

Damoiseaux JS, Rombouts SA, Barkhof F, Scheltens P, Stam CJ, Smith SM, Beckmann CF (2006): Consistent resting-state networks across healthy subjects. Proc Natl Acad Sci USA 103: 13848–13853.

De Luca M, Beckmann CF, De Stefano N, Matthews PM, Smith SM (2006): fMRI resting state networks define distinct modes of long-distance interactions in the human brain. Neuroimage 29:1359–1367.

Esposito F, Bertolino A, Scarabino T, Latorre V, Blasi G, Popolizio T, Tedeschi G, Cirillo S, Goebel R, Di Salle F (2006): Independent component model of the default-mode brain function: Assessing the impact of active thinking. Brain Res Bull 70:263–269.

Fox MD, Corbetta M, Snyder AZ, Vincent JL, Raichle ME (2006): Spontaneous neuronal activity distinguishes human dorsal and ventral attention systems. Proc Natl Acad Sci USA 103:10046–10051.

Fox MD, Snyder AZ, Vincent JL, Corbetta M, Van Essen DC, Raichle ME (2005): The human brain is intrinsically organized into dynamic, anticorrelated functional networks. Proc Natl Acad Sci USA 102:9673–9678.

Fransson P (2005): Spontaneous low-frequency BOLD signal fluctuations: An fMRI investigation of the resting-state default mode of brain function hypothesis. Hum Brain Mapp 26:15–29.

Fransson P (2006): How default is the default mode of brain function? Further evidence from intrinsic BOLD signal fluctuations. Neuropsychologia 44:2836–2845.

Friston K (1994): Functional and effective connectivity in neuroimaging: A synthesis. Hum Brain Mapp 2:56–78.

Gavrilescu M, Shaw ME, Stuart GW, Eckersley P, Svalbe ID, Egan GF (2002): Simulation of the effects of global normalization procedures in functional MRI. Neuroimage 17:532–542.

Gilbert SJ, Spengler S, Simons JS, Steele JD, Lawrie SM, Frith CD, Burgess PW (2006): Functional specialization within rostral prefrontal cortex (area 10): a meta-analysis. J Cogn Neurosci 18:932–948.

Goebel R, Roebroeck A, Kim DS, Formisano E (2003): Investigating directed cortical interactions in time-resolved fMRI data using vector autoregressive modeling and Granger causality mapping. Magn Reson Imaging 21:1251–1261.

Granger CWJ (1969): Investigating causal relations by econometric models and cross-spectral methods. Econometrica 37:424–438.

Greicius MD, Krasnow B, Reiss AL, Menon V (2003): Functional connectivity in the resting brain: A network analysis of the default mode hypothesis. Proc Natl Acad Sci USA 100:253–258.

Greicius MD, Menon V (2004): Default-mode activity during a passive sensory task: Uncoupled from deactivation but impacting activation. J Cogn Neurosci 16:1484–1492.

Greicius MD, Srivastava G, Reiss AL, Menon V (2004): Default-mode network activity distinguishes Alzheimer's disease from healthy aging: Evidence from functional MRI. Proc Natl Acad Sci USA 101:4637–4642.

Gusnard DA, Akbudak E, Shulman GL, Raichle ME (2001a): Medial prefrontal cortex and self-referential mental activity: Relation to a default mode of brain function. Proc Natl Acad Sci USA 98:4259–4264.

Gusnard DA, Raichle ME, Raichle ME (2001b): Searching for a baseline: Functional imaging and the resting human brain. Nat Rev Neurosci 2:685–694.

Hampson M, Driesen NR, Skudlarski P, Gore JC, Constable RT (2006): Brain connectivity related to working memory performance. J Neurosci 26:13338–13343.

Honey CJ, Kotter R, Breakspear M, Sporns O (2007): Network structure of cerebral cortex shapes functional connectivity on multiple time scales. Proc Natl Acad Sci USA 104:10240–10245.

Iacoboni M, Lieberman MD, Knowlton BJ, Molnar-Szakacs I, Moritz M, Throop CJ, Fiske AP (2004): Watching social interactions produces dorsomedial prefrontal and medial parietal BOLD fMRI signal increases compared to a resting baseline. Neuroimage 21:1167–1173.

Kelly AMC, Uddin LQ, Biswal BB, Castellanos FX, Milham MP (2007): Competition between functional brain networks mediates behavioral variability. Neuroimage in press.

Kennedy DP, Redcay E, Courchesne E (2006): Failing to deactivate: Resting functional abnormalities in autism. Proc Natl Acad Sci USA 103:8275–8280.

Lee AT, Glover GH, Meyer CH (1995): Discrimination of large venous vessels in time-course spiral blood-oxygen-level-dependent magnetic-resonance functional neuroimaging. Magn Reson Med 33:745–754.

Liang M, Zhou Y, Jiang T, Liu Z, Tian L, Liu H, Hao Y (2006): Widespread functional disconnectivity in schizophrenia with resting-state functional magnetic resonance imaging. Neuroreport 17:209–213.

Liu H, Liu Z, Liang M, Hao Y, Tan L, Kuang F, Yi Y, Xu L, Jiang T (2006): Decreased regional homogeneity in schizophrenia: A resting state functional magnetic resonance imaging study. Neuroreport 17:19–22.

Lou HC, Luber B, Crupain M, Keenan JP, Nowak M, Kjaer TW, Sackeim HA, Lisanby SH (2004): Parietal cortex and representation of the mental Self. Proc Natl Acad Sci USA 101:6827–6832.

Lundstrom BN, Ingvar M, Petersson KM (2005): The role of precuneus and left inferior frontal cortex during source memory episodic retrieval. Neuroimage 27:824–834.

Macey PM, Macey KE, Kumar R, Harper RM (2004): A method for removal of global effects from fMRI time series. Neuroimage 22:360–366.

Macrae CN, Moran JM, Heatherton TF, Banfield JF, Kelley WM (2004): Medial prefrontal activity predicts memory for self. Cereb Cortex 14:647–654.

Margulies DS, Kelly AM, Uddin LQ, Biswal BB, Castellanos FX, Milham MP (2007): Mapping the functional connectivity of anterior cingulate cortex. Neuroimage 37:579–588.

Mason MF, Norton MI, Van Horn JD, Wegner DM, Grafton ST, Macrae CN (2007): Wandering minds: The default network and stimulus-independent thought. Science 315:393–395.

McIntosh AR (2000): Towards a network theory of cognition. Neural Netw 13:861–870.

McKiernan KA, Kaufman JN, Kucera-Thompson J, Binder JR (2003): A parametric manipulation of factors affecting task-induced deactivation in functional neuroimaging. J Cogn Neurosci 15:394–408.

McKiernan KA, D'Angelo BR, Kaufman JN, Binder JR (2006): Interrupting the "stream of consciousness": an fMRI investigation. Neuroimage 29:1185–1191.

Miall RC, Robertson EM (2006): Functional imaging: Is the resting brain resting? Curr Biol 16:R998–R1000.

Mitchell JP, Heatherton TF, Macrae CN (2002): Distinct neural systems subserve person and object knowledge. Proc Natl Acad Sci USA 99:15238–15243.

Mitchell JP, Macrae CN, Banaji MR (2006): Dissociable medial prefrontal contributions to judgments of similar and dissimilar others. Neuron 50:655–663.

Nobre AC, Sebestyen GN, Gitelman DR, Mesulam MM, Frackowiak RS, Frith CD (1997): Functional localization of the system for visuospatial attention using positron emission tomography. Brain 120 (Part 3):515–533.

Nyberg L, McIntosh AR, Cabeza R, Nilsson LG, Houle S, Habib R, Tulving E (1996): Network analysis of positron emission tomography regional cerebral blood flow data: Ensemble inhibition during episodic memory retrieval. J Neurosci 16:3753–3759.

Raichle ME, MacLeod AM, Snyder AZ, Powers WJ, Gusnard DA, Shulman GL (2001): A default mode of brain function. Proc Natl Acad Sci USA 98:676–682.

Rizzolatti G (2005): The mirror neuron system and its function in humans. Anat Embryol (Berl) 210, 419–421.

Rizzolatti G, Craighero L (2004): The mirror-neuron system. Annu Rev Neurosci 27, 169–192.

Roebroeck A, Formisano E, Goebel R (2005): Mapping directed influence over the brain using Granger causality and fMRI. Neuroimage 25:230–242.

Saad ZS, Ropella KM, Cox RW, DeYoe EA (2001): Analysis and use of FMRI response delays. Hum Brain Mapp 13:74–93.

Seeley WW, Menon V, Schatzberg AF, Keller J, Glover GH, Kenna H, Reiss AL, Greicius MD (2007): Dissociable intrinsic connectivity networks for salience processing and executive control. J Neurosci 27:2349–2356.

Singer T, Seymour B, O'Doherty J, Kaube H, Dolan RJ, Frith CD (2004): Empathy for pain involves the affective but not sensory components of pain. Science 303:1157–1162.

Tian L, Jiang T, Wang Y, Zang Y, He Y, Liang M, Sui M, Cao Q, Hu S, Peng M, Zhuo Y (2006): Altered resting-state functional connec-

tivity patterns of anterior cingulate cortex in adolescents with attention deficit hyperactivity disorder. Neurosci Lett 400:39–43.

Uddin LQ, Kaplan JT, Molnar-Szakacs I, Zaidel E, Iacoboni M (2005): Self-face recognition activates a frontoparietal "mirror" network in the right hemisphere: An event-related fMRI study. Neuroimage 25:926–935.

Uddin LQ, Iacoboni M, Lange C, Keenan JP (2007): The self and social cognition: The role of cortical midline structures and mirror neurons. Trends Cogn Sci.

Vincent JL, Snyder AZ, Fox MD, Shannon BJ, Andrews JR, Raichle ME, Buckner RL (2006): Coherent spontaneous activity identifies a hippocampal-parietal memory network. J Neurophysiol 96:3517–3531.

Wang L, Zang Y, He Y, Liang M, Zhang X, Tian L, Wu T, Jiang T, Li K (2006): Changes in hippocampal connectivity in the early stages of Alzheimer's disease: Evidence from resting state fMRI. Neuroimage 31:496–504.

Weissman DH, Roberts KC, Visscher KM, Woldorff MG (2006): The neural bases of momentary lapses in attention. Nat Neurosci 9:971–978.

Wicker B, Ruby P, Royet JP, Fonlupt P (2003): A relation between rest and the self in the brain? Brain Res Brain Res Rev 43:224–230.

Zang YF, Yong H, Chao-Zhe Z, Qing-Jiu C, Man-Qiu S, Meng L, Li-Xia T, Tian-Zi J, Yu-Feng W (2007): Altered baseline brain activity in children with ADHD revealed by resting-state functional MRI. Brain Dev 29:83–91.